J Mol Model (2013) 19:5063–5073
DOI 10.1007/s00894-013-2000-z

ORIGINAL PAPER

DFT model cluster studies of O2 adsorption on hydrogenated titania sub-nanoparticles

Alexey S. Andreev · Vyacheslav N. Kuznetsov · Yuri V. Chizhov

Received: 21 June 2013 / Accepted: 8 September 2013 / Published online: 2 October 2013

Abstract In the present paper, we examine the general applicability of different TiO_2 model clusters to study of local chemical events on TiO_2 sub-nanoparticles. Our previous DFT study of TiO_2 activation through H adsorption and following deactivation by O_2 adsorption using small amorphous Ti_8O_{16} cluster were complemented by examination of rutile-type and spherical $Ti_{15}O_{30}$ nanoclusters. The obtained results were thoroughly compared with experimental data and results of related computational studies using other TiO_2 models including periodic structures. It turned out that all considered model TiO_2 model systems provide qualitatively similar results. It was shown that atomic hydrogen is adsorbed with negligible activation energy on surface O atoms, which is accompanied by the appearance of reduced Ti^{3+} species and corresponding localized band gap 3d-Ti states. Oxygen molecule is adsorbed on Ti^{3+} sites spontaneously forming molecular O_2^- species by capturing an extra electron of Ti^{3+} ion, which results in disappearance of Ti^{3+} species and corresponding band gap states. Calculated g-tensor values of Ti^{3+} and O_2^- species agree well with the results of EPR studies and do not depend on the used TiO_2 model cluster. Additionally, it was shown that the various cluster calculations provide results comparable with the calculations of periodic structures with respect to the modeling of chemical processes under study. As a whole, the present study approves the validity of molecular cluster approach to study of local chemical events on TiO_2 sub-nanoparticles.

Keywords Adsorption species · Atomic hydrogen · DFT study · g-factor · Molecular oxygen · Nanoclusters · Titanium dioxide

Introduction

At present, considerable efforts are devoted to synthesis, characterization and investigation of metal oxide nanoparticles. This trend has also embraced TiO_2 as the most promising environmental and pollution photocatalyst. Recent progress in synthesis, modifications, and applications of TiO_2 nanomaterials was the subject of some excellent reviews [1, 2].

Generally, TiO_2 particles with the size of 10 nm and smaller have been obtained by numerous methods. For example, Reyes-Coronado and co-workers have synthesized nanoparticles with anatase, rutile and brookite structures, using amorphous titania as a common starting material obtained by solution-phase methods [3]. In the case of anatase, the particle radius varies from 3 to 6 nm; rutile particles can be prepared with average radius between 5 and 15 nm; and for brookite the particle radius varies between about 5 and 10 nm. Dittert and co-workers have prepared stable nanoscaled titania from the molecular precursor titanium using a MicroJetReactor [4]. The measurements by dynamic light scattering showed that the size of the particles is distributed from 1 to 10 nm. Oskam and co-workers [5, 6] have reported the growth kinetics of TiO_2 nanoparticles synthesized from aqueous solution using titanium-(IV) isopropoxide as precursor. Transmission electron microscopy showed that average radius for as-prepared particles was 1.55 nm and increased to 1.95 nm with the temperature and time of the synthesis.

Specific surface area, surface-to-volume ratio and density of surface corner or edge sites of particles change significantly, when their size decreases to the nanometer or sub-nanometer scale. It is believed that such nano- or sub-nano-structured metal oxide materials can exhibit unique structural,

Electronic supplementary material The online version of this article (doi:10.1007/s00894-013-2000-z) contains supplementary material, which is available to authorized users.

A. S. Andreev · V. N. Kuznetsov · Y. V. Chizhov (✉)
V. A. Fock Institute of Physics, St. Petersburg State University, Ulyanovskaya Str. 1, St. Petersburg 198504, Russia
e-mail: yurichizhov@yandex.ru

electronic, and chemical properties. At present it is very important to understand how size decreasing and surface reconstruction affect chemical activity of TiO_2. Solution of this problem is the major challenge to quantum chemistry methods. Among different theoretical approaches implication of individual molecular $(TiO_2)_n$ clusters seems to be quite promising to study the local chemical events on the surface of TiO_2 sub-nanoparticles.

In a previous paper [7], we have studied atomic hydrogen adsorption and following molecular oxygen adsorption on TiO_2 using small amorphous Ti_8O_{16} model cluster. DFT calculations have shown that the sequence of two studied adsorption processes results in activation of cluster with formation of Ti^{3+} active sites followed by deactivation with disappearance of Ti^{3+} species and with concurrent appearance of new O_2^- ones. It was essential for us that, despite the small size of model cluster, this approach gave the results to be in a good agreement with general experimental regularities of both H plasma TiO_2 reduction and interaction of reduced TiO_2 with molecular oxygen. Nevertheless, the cluster is much smaller than those found normally in powders. It has atypical highly reactive under-coordinated terminal oxygen atoms and four-coordinated titanium ones, but does not have bulk-like six-coordinated Ti atoms and crystal-like ordered structure. This is a common problem of $(TiO_2)_n$ clusters. On the one hand, if the particles become small, their structure cannot be derived from the bulk. On the other hand, there is a great abundance of polymorphic forms of such particles. Therefore, the link between such small model clusters and real extended systems is not so obvious.

Considerable efforts of other authors have been devoted earlier to characterization of various $(TiO_2)_n$ structures of different sizes ($n = 1 – 68$) and shapes (amorphous, "truncated bulk" clusters, tubes and so on) via quantum chemical calculations [8–14]. The general conclusion is the following: for clusters with size less than ~1 nm there is no systematic relation between size, shape and properties such as band gaps, ionization potentials, electron affinity and so on. The aim of this paper is to study two times larger TiO_2 clusters with non-amorphous ordered structure in order to make sure that our results obtained earlier [7] are sustained to the choice of the model TiO_2 cluster. Based on the original work by Qu and Kroes who studied $(TiO_2)_n$ clusters with n from 10 to 16 [11], we chose two of the most proper $Ti_{15}O_{30}$ clusters. The first cluster represents a small rutile nanocrystal, so it differs from our recent model Ti_8O_{16} cluster both in size and in crystallinity degree. In our opinion it is suitable for modeling of the adsorption activity of steps, corners or edges on the surfaces of the TiO_2 nanoparticles. The second cluster has the ordered but non-crystal geometry structure with the spherical shape. The main feature of this cluster is the smallest energy gap between occupied and vacant levels in comparison with other clusters [11]. It was very interesting for us whether this feature and the specific spherical shape affects adsorption activity of cluster's atoms.

In the present work we examined both clusters and considered the sequence of atomic hydrogen and molecular oxygen adsorption as a "handy" chemical test. This choice was made for several reasons. Firstly, it allowed us to validate our previous results. Secondly, atomic adsorption of hydrogen is a well-studied process both experimentally and theoretically. Specifically, several papers were devoted to examination of chemical activity of different $(TiO_2)_n$ clusters and periodic titania structures using H adsorption as a probe [9, 13, 15], so we also have enough data to compare different TiO_2 model structures. Thirdly, the active O_2 adsorption on reduced TiO_2 is a well-known fact from experimental studies, but not from theoretical ones. To the best of our knowledge, there are only two studies dealt with the periodic calculations of O_2 adsorption on reduced titania [16, 17], but there are no studies at all where this process has been studied with the help of $(TiO_2)_n$ clusters. Therefore, it is a good object to study by using molecular cluster approach.

Computational details

The present DFT study was done using the GAUSSIAN 03 program [18]. The B3PW91 functional [19–25] was applied in all performed calculations, since it is the best choice for the g-tensor and band gap evaluation, as it has been recently shown for various semiconductors and inorganic compounds [26, 27]. Titanium atoms were represented by the LANL2DZ basis set [28] involved the Los Alamos effective core potential and double-ζ basis set. The standard full-electron 6-31G basis set [29] was used to describe O atoms. The reliability of similar B3LYP/LANL2DZ/D95 method has been demonstrated earlier by Qu and Kroes in the study of $(TiO_2)_n$ clusters ($n = 1$ to 16) [11]. To improve the description of atomic hydrogen adsorption we applied the 6-31++G** basis set [29] to H atoms which includes one polarized [30] and one diffused [31] function. Note that using diffuse and polarized functions on O atoms significantly increases computational time, but does not change significantly the final results [8, 13]. Geometry optimization procedures were carried out with the standard settings of the Gaussian 03 program and without any symmetry restrictions. The g-tensors of paramagnetic structures were calculated using GIAO method of Gaussian 03 program [18], and then obtained tensors were diagonalized.

The initial geometries of model $Ti_{15}O_{30}$ clusters considered in the present work were defined on the basis of rutile-type $(Ti_{15}O_{30})^R$ and spherical $(Ti_{15}O_{30})^S$ clusters examined by Qu and Kroes [11]. We re-optimized both clusters using the method described above and verified them on correspondence to the local minimum of energy by the harmonic vibrational frequency analysis. Re-optimized geometry structures of the

clusters are given in Supplementary material. The detailed describing of the geometry and electronic structure of these clusters are given in the Results section.

In the present study we examined the interaction of atomic H with only oxygen atoms of the clusters and considered the following adsorption of only one oxygen molecule on reduced titanium atoms. For this purpose an adsorbate was placed at a definite distance from a certain atom of the clusters followed by the full geometry optimization of the whole system and harmonic vibrational frequency analysis. In the case of atomic hydrogen adsorption every surface oxygen atom was considered as an adsorption site (the details are given in the Results section). The corresponding stable hydrogenated clusters were denoted as $(Ti_{15}O_{30}H)^R$ and $(Ti_{15}O_{30}H)^S$. The initial O–H distance was selected to be equal to 1.0 Å. In the case of molecular oxygen adsorption on hydrogenated clusters, only surface reduced Ti atoms were considered as adsorption sites (the details are given in the Results section). The corresponding stable clusters were denoted as $(Ti_{15}O_{30}H)^R$–O_2 and $(Ti_{15}O_{30}H)^S$–O_2. In this case the initial Ti–O_2 distances equaled to 1.5 Å. Note that both the linear and perpendicular fashions of O_2 adsorption were examined and the most stable one was chosen for further analysis.

The strength of H or O_2 adsorption was evaluated by adsorption energy E_{ads} according to the expression:

$$E_{ads}\left(X\middle/Y\right) = E(X) + E(Y) - E(Y\text{–}X),$$

where $E(X)$ is the energy of isolated adsorbate X (X=H or O_2) in the ground state, $E(Y)$ is the total energy of initial cluster Y (Y=$(Ti_{15}O_{30})^{R/S}$ or $(Ti_{15}O_{30}H)^{R/S}$) and $E(Y–X)$ is the total energy of the cluster with adsorbed reactant after geometry optimization. The positive value E_{ads} corresponds to exothermic adsorption.

Additionally we checked the presence of any energy barriers on the adsorption way to be sure that the reactions can occur. For this purpose the rigid (without geometry relaxation in each point) potential energy surface scan along the adsorption pathway was carried out. Specifically the adsorption activation energies E_{act} (the energy barriers) of adsorbate X (H or O_2) were evaluated from the profile of the total energy of an Y–X system (Y=$(Ti_{15}O_{30})^{R/S}$ or $(Ti_{15}O_{30}H)^{R/S}$) as a function of distance R(O–X) or R(Ti–X). The E_{act} values were given by the equation:

$$E_{act}\left(X\middle/Y\right) = E_{max}(Y\text{–}X) - E(Y) - E(X),$$

where E_{max}(Y–X) is the maximum of the total energy for the Y–X system on the energy profile.

Results

$Ti_{15}O_{30}$ clusters: geometry and electronic structure

The rutile-type $(Ti_{15}O_{30})^R$ cluster has C_{2v} symmetry and represents a small rutile nanocrystall. Assuming a half-spherical shape, the cluster's diameter equals to ~1.0 nm; see Fig. 1a. It is characterized by two bulk-like octahedral six-coordinated Ti(6), three five-coordinated Ti(5) and 10 four-coordinated Ti(4) atoms. It also contains seven three-coordinated O(3) and 23 bridging O(2) oxygen atoms. Due to symmetry reason, only six Ti atoms and 11 oxygen atoms are nonequivalent. Additionally, only ten oxygen and five titanium nonequivalent atoms are placed at the surface, i.e., are accessible to adsorption of any atoms and molecules.

The second $Ti_{15}O_{30}$ cluster has C_{2h} symmetry and spherical non-crystal shape with the diameter ~0.9 nm; see Fig. 1b. It is more stable than the rutile-type cluster being only at 0.298 eV lower in the total energy (or at 0.357 eV including zero point energy correction). The spherical cluster is characterized by one octahedral Ti(6) atom, eight five-coordinated Ti(5) and six four-coordinated Ti(4) titanium atoms; and also by four four-coordinated O(4), two three-coordinated O(3) and 24 bridging O(2) oxygen atoms. All O(4), O(3) and Ti(6) atoms are not accessible to adsorption of any atoms

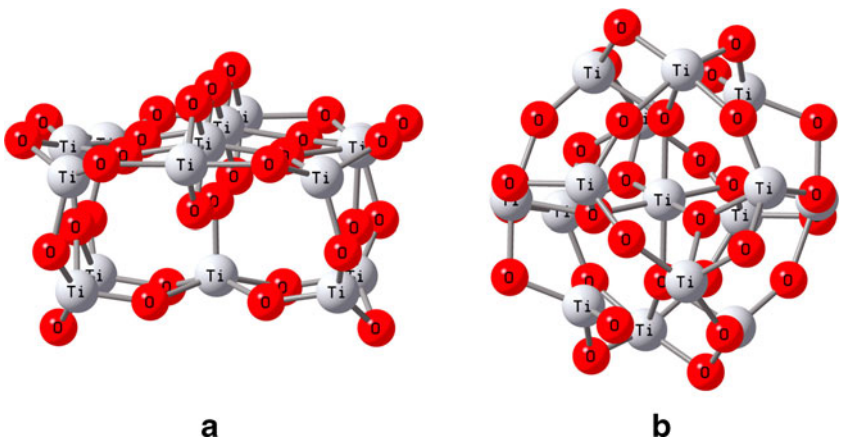

Fig. 1 Rutile-type $(Ti_{15}O_{30})^R$ (**a**) and spherical $(Ti_{15}O_{30})^S$ (**b**) clusters. The geometry structure of both clusters are based on the structure of rutile-type $(Ti_{15}O_{30})^R$ and spherical $(Ti_{15}O_{30})^S$ clusters examined by Qu and Kroes [ref. 11]

and molecules. At the same time, only seven of 24 surface oxygen and five of 14 titanium ones are nonequivalent. Thus, in both clusters there are enough adsorption sites with the different coordination types and different atomic surroundings in order to characterize the adsorption properties of the model particles statistically.

According to calculations, the singlet state of the clusters is the most stable. Figure 2 shows the energy diagrams of the frontier molecular orbitals (MO) of the clusters. The HOMOs and LUMOs consist generally of the O(2p) states and empty Ti(3d) atomic orbitals, respectively.

For rutile-type cluster both occupied and vacant MOs are found to be very close to each other within ~0.06 eV. Moreover, they are quite ***delocalized*** (for details, see Fig. 1S in Supplementary material). Figure 2a shows that between HOMO and LUMO levels there is an energy gap. Since frontier orbitals in the cluster have delocalized nature and lie close to each other, this gap quite resembles the band gap in crystals. Assuming this, the band gap of rutile-type $(Ti_{15}O_{30})^R$ cluster is equal to 4.28 eV.

The electronic structure of the spherical $(Ti_{15}O_{30})^S$ cluster is similar, but one exception takes place. Three lowest unoccupied levels in this cluster are separated from other LUMOs by 0.66 eV; see Fig. 2b. In terms of ligand field theory these vacant MOs can be referred to antibonding t_{2g}* orbitals. Unlike other vacant orbitals, these ones are quite ***localized*** and have large contribution (~70 %) from 3d orbitals of single octahedral Ti(6) atom (for details, see Fig. 1S in Supplementary material). Additionally note that these localized states are absent in both the small amorphous Ti_8O_{16} [7] and rutile-type $Ti_{15}O_{30}$ cluster. The HOMO-LUMO gap in $(Ti_{15}O_{30})^S$ cluster is considerably lower than that in the rutile-type cluster and equal to 3.14 eV. However, if we exclude these ***localized*** t_{2g}*-Ti(6) states from consideration, the gap between ***delocalized*** HOMO and LUMO, i.e., band gap, will be comparable with the band gap of the $(Ti_{15}O_{30})^R$ cluster and equal to 3.97 eV.

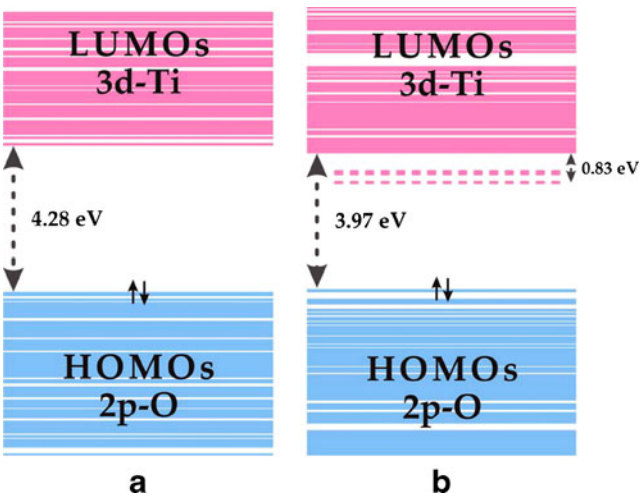

Fig. 2 Electronic structure diagrams for the rutile-like $(Ti_{15}O_{30})^R$ (**a**) and spherical $(Ti_{15}O_{30})^S$ (**b**) clusters; *dashed lines* indicates specific t_{2g}*-Ti(6) levels

Atomic hydrogen adsorption

The modeling of the atomic hydrogen adsorption on all nonequivalent surface oxygen atoms of both $Ti_{15}O_{30}$ clusters shows that the adsorption is always energetically preferable and results in formation of surface OH groups as expected. As a whole, ten stable hydrogenated rutile-type $(Ti_{15}O_{30}H)^R$ and seven spherical $(Ti_{15}O_{30}H)^S$ isomers were examined (see Fig. 2S and 3S in Supplementary material). The O–H bond length in all these isomers is generally about 1.0 Å; for comparison, the bond length of free hydroxide anion OH^- is equal to 0.964 Å [32]. The adsorption energies for rutile-type $(Ti_{15}O_{30}H)^R$ isomers are between 1.95 and 3.12 eV, while the lowest value corresponds to the adsorption on three-coordinated atom. Surprisingly, the adsorption energy values for spherical $(Ti_{15}O_{30}H)^S$ isomers are noticeably higher and found to be in the narrow range of 3.11 to 3.63 eV with the mean value 3.3 eV.

It was found that the activation energies of the H adsorption on bridging O atoms of both $Ti_{15}O_{30}$ clusters are negligible and on average equal to 0.1 eV. Figure 3 illustrates an example of the full energy profile for one of the hydrogenated $(Ti_{15}O_{30}H)^R$ isomers. In the case of the adsorption on O(3) atoms in rutile-type $(Ti_{15}O_{30})^R$, the E_{act} values are much higher, 0.7 and 0.9 eV, i.e., the adsorption is not preferable on these sites.

The calculations show that the ground state of all hydrogenated $Ti_{15}O_{30}H$ clusters is doublet. The spin density plots

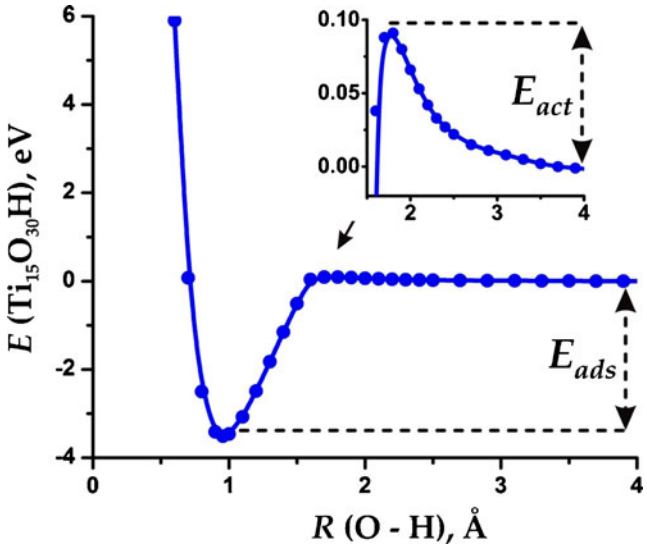

Fig. 3 Full energy profile for one of the hydrogenated $(Ti_{15}O_{30}H)^R$ isomers along the hydrogen adsorption pathway R(O–H); the adsorption energy E_{ads} is equal to 3.12 eV, the adsorption activation energy E_{act} is 0.11 eV; $E((Ti_{15}O_{30}H)^R)=0$ for R(O–H)=∞

indicate that an unpaired electron in each isomer is strongly localized on Ti atom. The localization of corresponding mulliken atomic spin density is near 100 %. It means that the metal atom was reduced from an initial +4 oxidized state into +3 one. In each of ten examined rutile-type $(Ti_{15}O_{30}H)^R$ isomers these reduced Ti^{3+} ions are adjacent to OH groups as shown in Fig. 4a, but it is not the case mostly for the spherical $(Ti_{15}O_{30}H)^S$ clusters. All examined $(Ti_{15}O_{30}H)^S$ isomers can be divided into two groups. In four isomers of the first group an unpaired electron is localized on the subsurface central Ti(6) atom (Fig. 4b), while Ti^{3+} ions in three isomers of the second group are again nearby OH groups. For clarity, the reduced Ti^{3+} ions in different isomers are indicated on the corresponding images in Figs. 2S and 3S in Supplementary material.

Ti^{3+} paramagnetic species resulted from the electron trapping can be characterized in terms of the g-factor that is a very convenient parameter for comparison with the experimental data. Despite that the electrons in different isomers are localized mainly on different Ti atoms, the difference of corresponding g-factors is surprisingly negligible. Table 1 shows the main components of the g-tensors calculated for rutile-type $(Ti_{15}O_{30}H)^R$ and spherical $(Ti_{15}O_{30}H)^S$ clusters and averaged over all isomers of each type. The left column contains the reference EPR data obtained by Berger and co-authors for the low-temperature H-plasma treated TiO_2 anatase nanoparticles [33].

The electronic structure analysis of reduced $Ti_{15}O_{30}H$ clusters shows that the reduced Ti^{3+} centers are responsible for presence of localized singly occupied 3d-Ti states near the middle of the band gap, see Fig. 5. The energy distance between Ti^{3+} levels and delocalized LUMO states in different rutile-type $(Ti_{15}O_{30}H)^R$ isomers ranges from 1.84 to 2.50 eV. At the same time, the band gaps of these isomers are quite similar and equal to ~4.3 eV. Note that the band gap of stoichiometric rutile-type $Ti_{15}O_{30}$ cluster is 4.28 eV. As the difference of the band gap values is negligible in comparison with the difference between energies of Ti^{3+} levels, in Fig. 5 we show the band gap equal to the mean value. The exact positions of Ti^{3+} levels and the band gap values for all calculated isomers are listed in Supplementary material, Table 1S.

As was mentioned above, there are two groups of reduced spherical clusters: with sub-surface and surface Ti^{3+} ions. The electronic structure diagram for hydrogenated clusters of the first group is shown in Fig. 5b. In this case an unpaired electron populates one of the localized vacant t_{2g}* orbitals of the subsurface octahedral Ti(6) atom. Remember that before the H adsorption these specific vacant states were placed at 0.66 – 0.83 eV lower than the other LUMO states (see Fig. 2b) and they are preferentially occupied when the cluster is reduced. As a result of adsorption, when the electron occupies one of three t_{2g}* levels, the resulting singly-occupied level stabilizes and takes up a new position in the gap at about 2.3 eV lower than the LUMO states, while two vacant t_{2g}* levels shift into the LUMO-zone. In isomers of the second group, where Ti^{3+} ions are located at the surface, the corresponding singly occupied 3d-Ti levels arise in the band gap, but the localized vacant t_{2g}* levels of the central Ti(6) atom remain untouched; see Fig. 5c.

The formation of OH groups and reduction of Ti atoms after H adsorption are accompanied mainly by the relatively small structure relaxation of the stoichiometric $Ti_{15}O_{30}$-core in hydrogenated clusters. In other words, the $Ti_{15}O_{30}$-cores of the hydrogenated isomers are similar to the initial stoichiometric clusters. Specifically, such structural relaxation results in elongation of all Ti^{3+}–O bonds by about 0.1 Å and all OH–Ti bonds by about 0.2 Å in comparison with the corresponding bonds in the initial clusters. However, there are some exceptions. The first is the one spherical $(Ti_{15}O_{30}H)^S$ isomer, where the coordination type of OH group does not correspond to that of the naked oxygen atom in the initial $(Ti_{15}O_{30})^S$ cluster. The second exception is the one rutile-type $(Ti_{15}O_{30}H)^R$ isomer, where H adsorption on three-coordinated oxygen atom causes significant structural changes of the $Ti_{15}O_{30}$-core. Nevertheless, these exceptions do not affect the results described above.

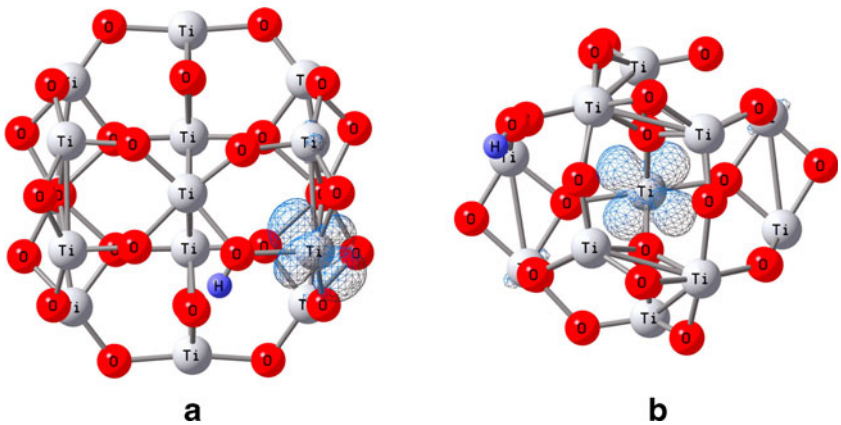

Fig. 4 Examples of hydrogenated $(Ti_{15}O_{30}H)^R$ (**a**) and $(Ti_{15}O_{30}H)^S$ (**b**) clusters; spin density of Ti^{3+} ions is shown as mesh

Table 1 Experimental and computed values of the main components of the g-tensors for Ti^{3+} centers. Experimental data were taken from ref [33]

	Experimental data [33]	Calculated values[a]	
		$(Ti_{15}O_{30}H)^R$	$(Ti_{15}O_{30}H)^S$
g_{xx}	1.992	1.991±0.006	1.990±0.003
g_{yy}	1.982	1.975±0.006	1.96±0.01
g_{zz}	1.960	1.96±0.01	1.952±0.005

[a] The average values are given together with the standard deviation. The exact Ti^{3+} g-tensor values for each $Ti_{15}O_{30}H$ isomer are presented in Supplementary material, Table 1S

Molecular oxygen adsorption on reduced clusters

It has been established theoretically that in reduced TiO_2 extra electrons can localize on many different Ti sites rather than on Ti atoms vicinal to the reductive defects such as hydroxyls, or O vacancies [34–38]. This leads to many different local energy minima structures, so the electron transport in such systems can occur via hopping of electrons from one Ti site to another with small activation energy (less than 0.3 eV) [34, 35, 39]. Thus, O_2 adsorption on reduced TiO_2 is possible on both specific Ti^{3+} sites and on many different Ti atoms with small activation energy. In the present work we considered only direct interaction/adsorption of molecular oxygen on surface Ti^{3+} sites vicinal to hydroxyls. For this purpose, we examined all available $Ti_{15}O_{30}H$ isomers with surface Ti^{3+} ions accessible to the adsorption of molecules. As a result we considered the adsorption on nine rutile-type $(Ti_{15}O_{30}H)^R$ and only three different $(Ti_{15}O_{30}H)^S$ isomers (see Fig. 2S and 3S in Supplementary material). As expected, the molecular oxygen always actively interacts with reduced Ti^{3+} sites. Figure 6 shows that the adsorbed molecule does not dissociate and remains in molecular form. Moreover, no energy barrier for this process was found, i.e., the adsorption can occur spontaneously. Note that the adsorption in perpendicular fashion atop titanium atoms is the most favorable.

It was found that the adsorption is accompanied by the complete transfer of the unpaired electrons from Ti^{3+} sites of hydrogenated clusters to the π^* orbital of the adsorbed O_2 molecule, as shown in Fig. 6. Moreover, localized singly occupied 3d-Ti gap states and corresponding paramagnetic Ti^{3+} centers disappear. As a result, the O_2^- paramagnetic species are formed, for which O–O bond length is larger by ~0.1 Å than that of the free O_2 molecule. These new paramagnetic centers can be characterized also by new values of g-tensor, as shown in Table 2. Note that the difference of the g-factors calculated for different $(Ti_{15}O_{30}H)$–O_2 isomers is again surprisingly negligible.

In comparison with the H adsorption the O_2 adsorption is accompanied by a noticeable structural relaxation of the stoichiometric $Ti_{15}O_{30}$-core. Specifically, the structural flexibility of two rutile-type $(Ti_{15}O_{30}H)^R$ isomers results in a change of the Ti sites coordination from four-coordinated to new three-coordinated. Additionally, the relaxation of one of the spherical $(Ti_{15}O_{30}H)^S$ isomers results in the transformation of five-coordinated Ti site to four-coordinated one. The strong relaxation occurs in another two rutile-type isomers, where five-coordinated Ti sites are transformed to three-coordinated ones.

In this connection, it should be noted that if the relaxation energy contribution in E_{ads} becomes noticeable the adsorption energy calculation also gives noticeably higher values, which cannot be directly compared with others. Therefore, we present here the values only for five $(Ti_{15}O_{30}H)^R$–O_2 rutile-type and two spherical $(Ti_{15}O_{30}H)^S$–O_2 isomers, where the structural relaxation is not high. The information about other isomers is given in Supplementary material, Table 2S. The estimation of the adsorption energies for rutile-type $(Ti_{15}O_{30}H)^R$–O_2 isomers shows that $E_{ads}(O_2)$ values are in the range from 1.2 to 2.1 eV. Note that the lowest value

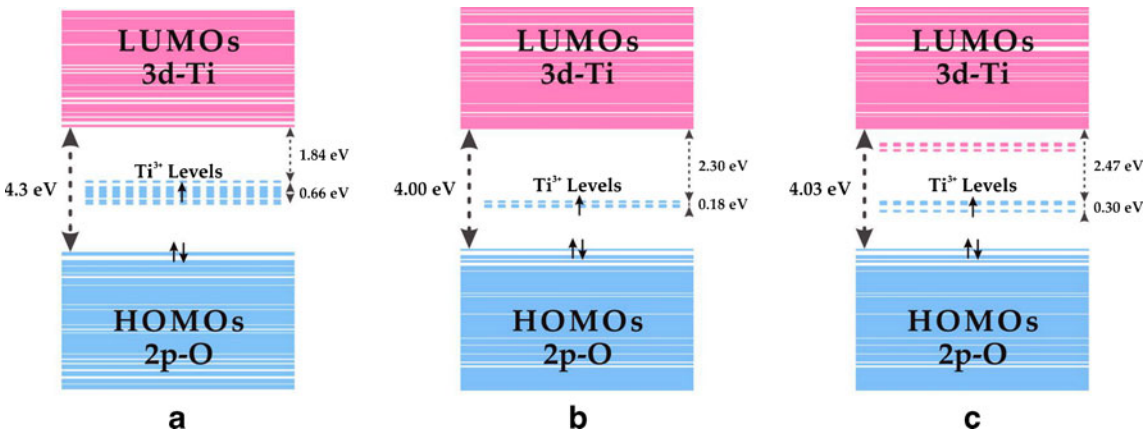

Fig. 5 Electronic structure diagrams for hydrogenated rutile $(Ti_{15}O_{30}H)^R$ (**a**) and two types of spherical $(Ti_{15}O_{30}H)^S$ clusters (**b** and **c**); *dashed lines with arrow* show the levels corresponding to Ti^{3+} ions in different clusters; *dashed lines without arrow* (**c**) indicate specific localized vacant t_{2g}*-Ti(6) levels

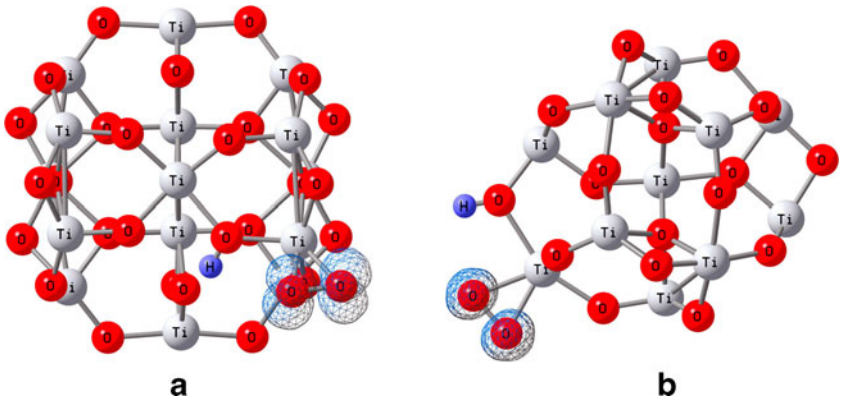

Fig. 6 Examples of the $(Ti_{15}O_{30}H)^{R}$–O_2 (**a**) and $(Ti_{15}O_{30}H)^{S}$–O_2 (**b**) clusters; spin density of O_2^- species is shown as mesh

corresponds to the single isomer with the five-coordinated adsorptive site. The $E_{ads}(O_2)$ values for the other four isomers with four-coordinated Ti sites range from 1.4 to 2.0 eV with the mean value equals to 1.8 eV. Surprisingly, but the energies for spherical $(Ti_{15}O_{30}H)^{S}$ isomers are higher again: 1.81 and 1.86 eV for adsorption on five-coordinated sites.

Discussion

Despite the differences between the $Ti_{15}O_{30}$ model clusters used in the present study and the Ti_8O_{16} used in our previous one [7], they give qualitatively the same results. Let us summarize them:

(1) The interaction between atomic hydrogen and surface oxygen atoms of the clusters results in the formation of stable OH groups.
(2) The activation energy of this process is generally low, ~0.1 eV.
(3) Every hydrogen atom adsorption event results in the reduction of one titanium atom from +4 to +3 oxidation state and in the appearance of one corresponding localized singly occupied 3d-Ti state in the middle of the clusters' band gap.
(4) Ti^{3+} sites of the reduced clusters can spontaneously adsorb the molecular oxygen yielding the stable adsorbed molecular O_2^- species.
(5) After the molecular oxygen adsorption, Ti^{3+} centers and corresponding localized singly occupied 3d-Ti states in the clusters' band gap disappear.

Table 2 Experimental and computed values of the main components of the g-tensors for O_2^- species. Experimental data were taken from ref [40] and [41]

	Experimental data		Computed values[a]	
	Berger et al. [40]	Komaguchi et al. [41]	$(Ti_{15}O_{30}H)^{R}$–O_2	$(Ti_{15}O_{30}H)^{S}$–O_2
g_{xx}	2.0033	2.003	2.0031±0.0004	2.00331±0.00004
g_{yy}	2.0096	2.010	2.0107±0.0001	2.0109±0.0001
g_{zz}	2.0248	2.023	2.024±0.003	2.0214±0.0004

[a] The average values are given together with the standard deviation. The exact O_2^- g-tensor values for each $(Ti_{15}O_{30}H)$–O_2 isomer are listed in Supplementary material, Table 2S

These results agree with other experimental and theoretical studies very well. For instance, the various *ab-initio* studies have shown that the adsorbed or interstitial atomic hydrogen donates the extra electrons to TiO_2 that is accompanied by the reduction of Ti^{4+} ions to Ti^{3+} ones [9, 13, 34, 42–45]. Berger and co-authors have reported [33] that the low-temperature (at T=77 K) H plasma treatment of TiO_2 nanoparticles results in the spontaneous adsorption of the atomic hydrogen at the TiO_2 surface that indicates the insignificant activation energy of the adsorption. Additionally, the authors have reported that the hydrogenated samples are characterized by the blue color and the EPR signal with g_{xx}=1.992, g_{yy}=1.982, and g_{zz}=1.960 assigned to the Ti^{3+} ions. Note that it is common knowledge that the blue or dark blue color is the main feature of the reduced TiO_2 specimens and corresponds to their dominant optical absorption at $h\nu$<2 eV [46 and references therein]. Earlier, optical and EPR spectral studies allowed to assign the red and NIR absorption also to Ti^{3+} defect sites [33, 41, 47, 48].

It is known that the surface and subsurface Ti^{3+} sites in turn actively interact with the molecular oxygen. Such interaction results in the disappearance of these sites and the appearance of adsorbed O_2^- species [41, 49–52]. At the same time the disappearance of Ti^{3+} ions results in the strong decrease of the optical absorption in the red and NIR region and, consequently, in the blue color vanishing. In such cases the color of reduced samples is changed from blue to white or to yellow [41, 50, 53]. Furthermore, Komaguchi and co-authors have reported [41] that exposure of reduced rutile sample to O_2 at room temperature produced significant bleaching in the red

Table 3 Adsorption energies E_{ads}(H) and activation energies E_{act}(H) of H adsorption, band gap values E_{gap}(H) of hydrogenated clusters, positions of Ti^{3+} levels in the clusters' band gaps $E(Ti^{3+})$, g-tensor values of Ti^{3+} paramagnetic centers, energies of O_2 adsorption $E_{ads}(O_2)$ on reduced Ti sites of hydrogenated clusters, and g-tensor values of O_2^- species. All values are given for different model TiO_2 clusters. The data for Ti_8O_{16} cluster were taken from ref [7]. The E_{ads} and E_{act} values are given separately for isomers with adsorptive sites having different coordination number, which is specified in parentheses. The averaged values are given together with the standard deviation. The complete information is presented in Supplementary material, Table 1S and Table 2S

	Ti_8O_{16} [7]	$(Ti_{15}O_{30})^R$	$(Ti_{15}O_{30})^S$
E_{ads}(H)[a]	O(1): 2.9; 3.5 eV[b]	–	–
	O(2): 2.3 – 2.9 eV	O(2): 2.4 – 3.1 eV	O(2): 3.1 – 3.6 eV
	O(3): 2.1 eV[b]	O(3): 2.0 eV[b]	–
E_{act}(H)	O(1,2): 0.09 – 0.25 eV	O(2): 0.07 – 0.19 eV	O(2): 0.06 – 0.14 eV
	O(3): 0.72; 0.74 eV[b]	O(3): 0.68; 0.91 eV[b]	–
	O(4): 1.20 eV[b]	–	–
E_{gap}(H)	4.2±0.1 eV	4.3±0.1 eV	4.01±0.04 eV
$E(Ti^{3+})$	1.7 – 2.8 eV	1.8 – 2.5 eV	2.3 – 2.8 eV
g-tensor (Ti^{3+})	g_{xx}=1.992±0.003	g_{xx}=1.991±0.006	g_{xx}=1.990±0.003
	g_{yy}=1.979±0.004	g_{yy}=1.975±0.006	g_{yy}=1.96±0.01
	g_{zz}=1.957±0.008	g_{zz}=1.96±0.01	g_{zz}=1.952±0.005
$E_{ads}(O_2)$[a]	Ti(4): 1.4 – 2.0 eV	Ti(4): 1.4 – 2.1 eV	–
	Ti(5): 0.9 – 1.2 eV	Ti(5): 1.21 eV[b]	Ti(5): 1.81; 1.86 eV[b]
g-tensor (O_2^-)	g_{xx}=2.004±0.002	g_{xx}=2.0031±0.0004	g_{xx}=2.00331±0.00004
	g_{yy}=2.009±0.002	g_{yy}=2.0107±0.0001	g_{yy}=2.0109±0.0001
	g_{zz}=2.05±0.02	g_{zz}=2.024±0.003	g_{zz}=2.0214±0.0004

[a] The values are given only for those isomers, where the relatively small structural relaxation occurred after H or O_2 adsorption; for details see the Results section

[b] Only one or two values were obtained as a result of calculations

and NIR region with the strong decreasing of the Ti^{3+} EPR signal and with the concurrent appearance of the new signal with g_{xx}=2.003, g_{yy}=2.010, and g_{zz}=2.023 attributed to adsorbed O_2^-.

The quantitative results of the present calculations need to be discussed separately. Table 3 summarizes the adsorption energies of hydrogen and oxygen, the positions of Ti^{3+} electronic gap states and the main components of the Ti^{3+} and O_2^- g-tensors calculated with the using of the different model TiO_2 clusters. As can be seen, the rutile-type $(Ti_{15}O_{30})^R$ cluster and small amorphous Ti_8O_{16} cluster give all values to be quite similar. It applies also to the spherical $(Ti_{15}O_{30})^S$ cluster, with exception to the energies of H and O_2 adsorption.

Taking together our previous results and the results of other theoretical studies it was found that the energy of the atomic hydrogen adsorption correlates with the coordination type of resulted OH groups: the energy decreases with the increasing of the coordination number of the OH group. Figure 7 shows the adsorption energies calculated by us for $(Ti_{15}O_{30})^R$ and Ti_8O_{16} clusters, by Calatayud and Minot for different $(TiO_2)_n$ clusters (n=1 to 24) [9] and for rutile/anatase surfaces [9, 15], and by Syzgantseva with co-authors for different $(TiO_2)_n$ clusters (n=1 to 10) [13]. It should be emphasized that these values are evidently in the same ranges despite the great difference between the TiO_2 model systems (especially the clusters and crystal surfaces) and the computational methods. For example, some values (2.52 eV for the adsorption on

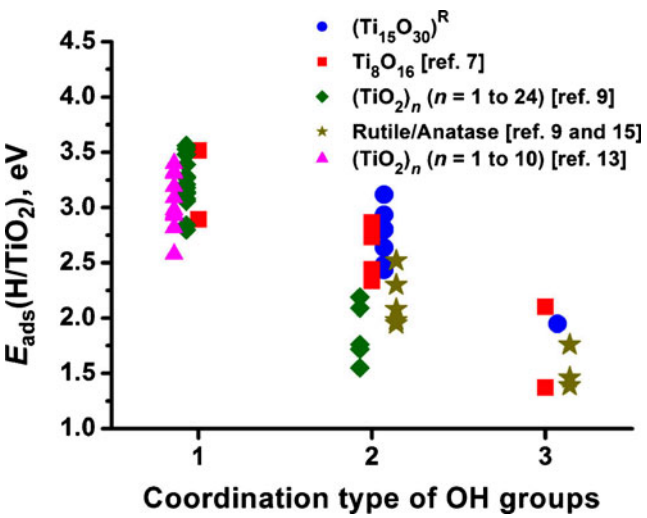

Fig. 7 The energies of the H adsorption (E_{ads}) calculated for different TiO_2 models studied in the present and other theoretical works [7, 9, 13, 15]. The values from the present work are given only for those isomers, where the relatively small structural relaxation occurred after H adsorption; for details see the Results section

bridging oxygen atoms and 1.76 eV for three-coordinated ones) were obtained for the full-covered rutile surface by the slab calculations using the PW91 GGA DFT approach with a plane-wave basis set [15]. In contrary, the adsorption of only one hydrogen atom on one terminal oxygen atom, for example, of the $Ti_{10}O_{20}$ cluster was simulated using hybrid B3LYP method with the LANL2DZ/6-31+G* basis sets [13]. Additionally note that the large variation of the energy values is very typical for cluster models. On the one hand, we found the values to be in the wide ranges examining the variety of different hydrogenated isomers of the same size. On the other hand, no systematic relation between the size of the cluster and the adsorption energy values has been found by the other authors [9, 13]. Thus, we suppose that the adsorption activity of the TiO_2 particles is determined mainly by the ***local atomic surroundings*** of the adsorption site, but not by the general characteristics such as the size of particle. In this connection, the spherical $(Ti_{15}O_{30})^S$ cluster becomes ever more atypical, since the energy values computed for this cluster are considerably higher than for other TiO_2 clusters independently on the adsorption site. Probably, this is due to the specific spherical shape of the cluster that is quite unusual to other clusters mentioned above. Thus, the geometry structure of the model cluster can significantly affect its adsorption activity and should be taken into account in the modeling of TiO_2 nanoparticles and their properties.

To the best of our knowledge, only two DFT studies dealt with the quantitative description of the O_2 adsorption at the reduced TiO_2 surface [16, 17]. Both studies were done at a similar theoretical level and give close energies for the O_2 adsorption on Ti sites of the reduced rutile surface with OH groups (the OH coverage was near 0.1; one OH group per one O_2 molecule). Unfortunately, only five-coordinated Ti sites were examined in both studies, so the quantitative comparison of the values is limited. Figure 8 shows the values obtained in these studies together with ours. As can be seen, the energies of the O_2 adsorption correlate with the coordination type of the adsorptive Ti sites. Furthermore, the values for Ti(5) atoms obtained for different reduced TiO_2 models are close. However, in this case the spherical reduced $(Ti_{15}O_{30}H)^S$ clusters again demonstrate the exception (see Table 3).

The comparison of optical experimental data with calculated band gap values and positions of defect gap states is an important and often discussed problem in TiO_2 studies and especially in studies of clusters. It is reasonable to give some important comments on this question. Firstly, it is known that the conventional HOMO-LUMO gaps may overestimate the optical band gaps of TiO_2 nanoparticles due to the multiconfiguration nature of the excited-state wave functions of the clusters [11]. Secondly, the calculated band gaps of the TiO_2 clusters (Ti_8O_{16} – 4.04 eV [7], $(Ti_{15}O_{30})^R$ – 4.28 eV, $(Ti_{15}O_{30})^S$ – 3.97 eV) exceed ones of the rutile and anatase (3.0 and ~3.2 eV, respectively [49]) rather noticeably only

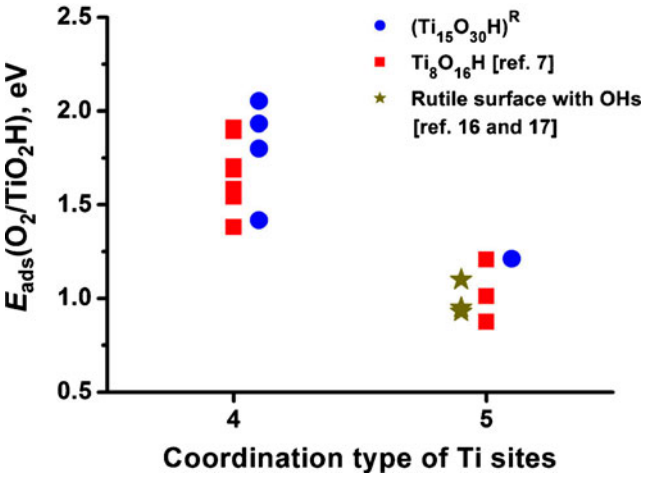

Fig. 8 The energies of the O_2 adsorption (E_{ads}) on reduced Ti sites calculated for different reduced TiO_2 models studied in the present and other theoretical works [7, 16, 17]. The values from the present work are given only for those isomers, where the relatively small structural relaxation occurred after O_2 adsorption; for details see the Results section

when compared with the band gaps of the single crystals. However, it is commonly known that there is a blue shift of optical absorption thresholds of nanoscale particles due to the quantum confinement. For TiO_2 the optical band gap increasing was estimated to be about 0.6 eV when the particles' radius decreases down to 1 nm [1, 49]. Thus, the excess of the calculated band gaps for clusters in comparison with the crystals demonstrates correct tendency. Thirdly, the positions of Ti^{3+} states in the clusters' band gaps (see Table 3) differ from the experimental maxima of the bands related with Ti^{3+} defect species in the single crystal absorption spectra ($h\nu_{max}$ at 1.5 – 1.7 and ~1.2 eV [46 and references herein]. At the same time both the calculated and experimental positions of Ti^{3+} states correspond qualitatively to the near-middle band gap levels, since they lie around 2.4 eV for clusters and 1.5 eV for crystals. Finally, the DFT has some shortcomings in the correct description of the TiO_2 electronic structure and especially of the defect gap states, which is the special debatable problem in various periodic calculations studies [44, 45]. Nevertheless, as was shown above, DFT is widely accepted to study of TiO_2 surface chemistry.

The computed g-tensor values of Ti^{3+} and O_2^- paramagnetic species in all studied clusters are found to be well reproducible quantitative characteristics. Furthermore, as can be seen from Tables 1 and 2, these values are very close to the ones obtained in EPR studies. Therefore, g-tensors computed in TiO_2 cluster model provide a reliable representation of the experimentally observed paramagnetic species in TiO_2 and can be used to support EPR studies. In this connection, it should be noted that in contrast to H and O_2 adsorption energies g-tensors turned out to be surprisingly almost insensitive to local atomic surroundings of paramagnetic centers. In our opinion, it indicates that the EPR analysis can distinguish

the differences between chemical environment of paramagnetic centers in TiO_2 only in highly ordered rigid structures like single crystals but not in small flexible nanoparticles.

Conclusions

In the present work we aimed to analyze the significance of the choice of model $(TiO_2)_n$ clusters to studies of simple chemical processes on the surface of titania sub-nanoparticles. The modeling results of H adsorption and following O_2 adsorption obtained for rutile-like and spherical $Ti_{15}O_{30}$ clusters were compared with ones for the small amorphous Ti_8O_{16} cluster, experimental data and the results of other related quantum-chemical studies. It was shown that various model $(TiO_2)_n$ clusters with different sizes and shapes provide the results in qualitative agreement with the experimental ones. Specifically they represent the appearance of reduced Ti^{3+} species with corresponding band gap localized 3d-Ti states after H adsorption and their disappearance after O_2 adsorption with the formation of O_2^- species. The calculated g-tensor values are found to be reliable quantitative characteristics of paramagnetic species in TiO_2, since they are sustained to the choice of model cluster and agree with the results of EPR studies. Comparative analysis of calculated adsorption energies show that the atypical geometry and electronic structure of the model cluster, namely $(Ti_{15}O_{30})^S$, can significantly affect its adsorption activity. Taking in general the cluster studies provide results comparable with the periodic calculations with respect to the modeling of chemical processes. In this connection, the clusters with crystal-like structures seem to be the most plausible models to further studies of both dark and photo induced chemical reactions on the surface of the TiO_2 sub-nanoparticles.

Acknowledgments The authors thank Prof. Alexei Emeline and Prof. Vladimir Ryabchuk for fruitful discussions. The present work was supported by Russian Foundation of Basic Research (Grant 10-03-00638-a) and St. Petersburg State University (Grant 11.37.25.2011). Computational resources were provided by Service of Informational Technologies of St. Petersburg State University (St. Petersburg, Russia).

References

1. Chen X, Mao SS (2007) Titanium dioxide nanomaterials: synthesis, properties, modifications, and applications. Chem Rev 107:2891–2959. doi:10.1021/cr0500535
2. Banerjee A (2011) The design, fabrication, and photocatalytic utility of nanostructured semiconductors: focus on TiO2-based nanostructures. Nanotechnol Sci Appl 4:35–65. doi:10.2147/NSA.S9040
3. Reyes-Coronado D, Rodríguez-Gattorno G, Espinosa-Pesqueira ME et al (2008) Phase-pure TiO2 nanoparticles: anatase, brookite and rutile. Nanotechnol 19:145605. doi:10.1088/0957-4484/19/14/145605
4. Dittert B, Gavrilović A, Schwarz S et al (2011) Phase content controlled TiO2 nanoparticles using the MicroJetReactor technology. J Eur Ceram Soc 31:2475–2480. doi:10.1016/j.jeurceramsoc.2011.01.015
5. Oskam G, Hu Z, Penn RL et al (2002) Coarsening of metal oxide nanoparticles. Phys Rev E Stat Nonlinear Soft Matter Phys 66:011403. doi:10.1103/PhysRevE.66.011403
6. Oskam G, Nellore A, Penn RL, Searson PC (2003) The growth kinetics of TiO2 nanoparticles from titanium(IV) alkoxide at high water/titanium ratio. J Phys Chem B 107:1734–1738. doi:10.1021/jp021237f
7. Andreev AS, Kuznetsov VN, Chizhov YV (2012) Atomic hydrogen activated TiO2 nanocluster: DFT calculations. J Phys Chem C 116:18139–18145. doi:10.1021/jp3009805
8. Calatayud M, Maldonado L, Minot C (2008) Reactivity of (TiO2)n clusters (n=1−10): probing gas-phase acidity and basicity properties. J Phys Chem C 112:16087–16095. doi:10.1021/jp802851q
9. Calatayud M, Minot C (2009) Is there a nanosize for the activity of TiO2 compounds? J Phys Chem C 113:12186–12194. doi:10.1021/jp901465q
10. Lundqvist MJ, Nilsing M, Persson P, Lunell S (2006) DFT study of bare and dye-sensitized TiO2 clusters and nanocrystals. Int J Quantum Chem 106:3214–3234. doi:10.1002/qua.21088
11. Qu Z-W, Kroes G-J (2007) Theoretical study of stable, defect-free (TiO2)n nanoparticles with n=10–16. J Phys Chem C 111:16808–16817. doi:10.1021/jp073988t
12. Qu Z-W, Kroes G-J (2006) Theoretical study of the electronic structure and stability of titanium dioxide clusters (TiO2)n with n=1–9. J Phys Chem B 110:8998–9007. doi:10.1021/jp056607p
13. Syzgantseva OA, Gonzalez-Navarrete P, Calatayud M et al (2011) Theoretical Investigation of the Hydrogenation of (TiO2)n Clusters (n=1–10). J Phys Chem C 115:15890–15899. doi:10.1021/jp2050349
14. Qu Z-W, Zhu H (2010) Do anionic titanium dioxide nano-clusters reach bulk band Gap? a density functional theory study. J Comput Chem 31:2038–2045. doi:10.1002/jcc
15. Yin X-L, Calatayud M, Qiu H et al (2008) Diffusion versus desorption: complex behavior of H atoms on an oxide surface. ChemPhysChem 9:253–256. doi:10.1002/cphc.200700612
16. Deskins NA, Rousseau R, Dupuis M (2010) Defining the role of excess electrons in the surface chemistry of TiO2. J Phys Chem C 114:5891–5897. doi:10.1021/jp101155t
17. Chrétien S, Metiu H (2008) Enhanced adsorption energy of Au1 and O2 on the stoichiometric TiO2(110) surface by coadsorption with other molecules. J Chem Phys 128:044714. doi:10.1063/1.2829405
18. Frisch MJ, Trucks GW, Schlegel HB et al. (2003) Gaussian 03, Revision B.05
19. Becke AD (1993) Density-functional thermochemistry. III. The role of exact exchange. J Chem Phys 98:5648
20. Vosko SH, Wilk L, Nusair M (1980) Accurate spin-dependent electron liquid correlation energies for local spin density calculations: a critical analysis. Can J Phys 58:1200–1211. doi:10.1139/p80-159
21. Perdew JP, Chevary JA, Vosko SH et al (1992) Atoms, molecules, solids, and surfaces: Applications of the generalized gradient approximation for exchange and correlation. Phys Rev B: Condens Matter Mater Phys 46:6671–6687. doi:10.1103/PhysRevB.46.6671
22. Burke K, Perdew JP, Wang Y (1998) Derivation of a generalized gradient approximation: the PW91 density functional. In: Dobson JF, Vignale G, Das MP (eds) Electron. Density Funct. Theory: Recent Prog. New Dir. Plenum Press, New York, pp 81–111
23. Perdew JP (1991) Unified theory of exchange and correlation beyond the local density approximation. In: Ziesche P, Eschrig H (eds) Electronic structure of solids. Akademie Verlag, Berlin, pp 11–20
24. Perdew JP, Chevary JA, Vosko SH et al (1993) Erratum: atoms, molecules, solids, and surfaces: applications of the generalized

gradient approximation for exchange and correlation. Phys Rev B: Condens Matter Mater Phys 48:4978. doi:10.1103/PhysRevB.48.4978.2
25. Perdew JP, Burke K, Wang Y (1996) Generalized gradient approximation for the exchange-correlation hole of a many-electron system. Phys Rev B: Condens Matter Mater Phys 54:16533–16539. doi:10.1103/PhysRevB.54.16533
26. Xiao H, Tahir-Kheli J, Goddard WAI (2011) Accurate band gaps for semiconductors from density functional theory. J Phys Chem Lett 2:212–217. doi:10.1021/jz101565j
27. Kaupp M, Reviakine R, Malkina OL et al (2002) Calculation of electronic g-tensors for transition metal complexes using hybrid density functionals and atomic meanfield spin-orbit operators. J Comput Chem 23:794–803. doi:10.1002/jcc.10049
28. Hay JP, Wadt WR (1985) Ab initio effective core potentials for molecular calculations. Potentials for K to Au including the outermost core orbitals. J Chem Phys 82:299
29. Hehre WJ, Ditchfield R, Pople JA (1972) Self—consistent molecular orbital methods. XII. Further extensions of Gaussian—type basis sets for use in molecular orbital studies of organic molecules. J Chem Phys 56:2257
30. Hariharan PC, Pople JA (1973) The influence of polarization functions on molecular orbital hydrogenation energies. Theor Chim Acta 28:213
31. Clark T, Chandrasekhar J, Spitznagel GW, Schleyer PVR (1983) Efficient diffuse function-augmented basis sets for anion calculations. III. The 3-21+G basis set for first-row elements, Li-F. J Comput Chem 4:294–301. doi:10.1002/jcc.540040303
32. NIST (2011) Computational Chemistry Comparison and Benchmark Database. Release 15b. http://cccbdb.nist.gov/
33. Berger T, Diwald O, Knözinger E et al (2007) Hydrogen activation at TiO2 anatase nanocrystals. Chem Phys 339:138–145. doi:10.1016/j.chemphys.2007.06.021
34. Deskins NA, Rousseau R, Dupuis M (2009) Localized electronic states from surface hydroxyls and polarons in TiO2 (110). J Phys Chem C 113:14583–14586. doi:10.1021/jp9037655
35. Deskins NA, Rousseau R, Dupuis M (2011) Distribution of Ti3+ surface sites in reduced TiO2. J Phys Chem C 115:7562–7572. doi:10.1021/jp2001139
36. Morgan BJ, Watson GW (2007) A DFT+U description of oxygen vacancies at the TiO2 rutile (110) surface. Surf Sci 601:5034–5041. doi:10.1016/j.susc.2007.08.025
37. Morgan BJ, Watson GW (2010) Intrinsic n-type defect formation in TiO2: a comparison of rutile and anatase from GGA+U calculations. J Phys Chem C 114:2321–2328. doi:10.1021/jp9088047
38. Helali Z, Markovits A, Minot C, Abderrabba M (2012) First-row transition metal atoms adsorption on rutile TiO2(110) surface. Struct Chem 23:1309–1321. doi:10.1007/s11224-012-0058-3
39. Deskins NA, Dupuis M (2007) Electron transport via polaron hopping in bulk TiO2: a density functional theory characterization. Phys Rev B 75:195212. doi:10.1103/PhysRevB.75.195212
40. Berger T, Sterrer M, Diwald O, Knözinger E (2005) Charge trapping and photoadsorption of O2 on dehydroxylated TiO2 nanocrystals-an electron paramagnetic resonance study. ChemPhysChem 6:2104–2112. doi:10.1002/cphc.200500161
41. Komaguchi K, Maruoka T, Nakano H et al (2010) Electron-Transfer Reaction of Oxygen Species on TiO2 Nanoparticles Induced by Sub-band-gap Illumination. J Phys Chem C 114:1240–1245. doi:10.1021/jp909678e
42. Leconte J, Markovits A, Skalli MK et al (2002) Periodic ab initio study of the hydrogenated rutile TiO2(110) surface. Surf Sci 497:194–204. doi:10.1016/S0039-6028(01)01477-7
43. Di Valentin C, Pacchioni G, Selloni A (2006) Electronic structure of defect states in hydroxylated and reduced rutile TiO2(110) surfaces. Phys Rev Lett 97:166803. doi:10.1103/PhysRevLett.97.166803
44. Finazzi E, Di Valentin C, Pacchioni G, Selloni A (2008) Excess electron states in reduced bulk anatase TiO2: comparison of standard GGA, GGA+U, and hybrid DFT calculations. J Chem Phys 129:154113. doi:10.1063/1.2996362
45. Di Valentin C, Pacchioni G, Selloni A (2009) Reduced and n-Type Doped TiO2: Nature of Ti3+ Species. J Phys Chem C 113:20543–20552. doi:10.1021/jp9061797
46. Kuznetsov VN, Serpone N (2009) On the origin of the spectral bands in the visible absorption spectra of visible-light-active TiO2 specimens analysis and assignments. J Phys Chem C 113:15110–15123. doi:10.1021/jp901034t
47. Khomenko VM, Langer K, Rager H, Fett A (1998) Electronic absorption by Ti3+ ions and electron delocalization in synthetic blue rutile. Phys Chem Miner 25:338–346. doi:10.1007/s002690050124
48. Sekiya T, Yagisawa T, Kamiya N et al (2004) Defects in anatase TiO2 single crystal controlled by heat treatments. J Phys Soc Jpn 73:703–710. doi:10.1143/JPSJ.73.703
49. Henderson MA (2011) A surface science perspective on TiO2 photocatalysis. Surf Sci Rep 66:185–297. doi:10.1016/j.surfrep.2011.01.001
50. Kuznetsov VN, Krutitskaya TK (1996) Nature of color centers in reduced titanium dioxide. Kinet Catal 37:446
51. Henderson MA, Epling WS, Perkins CL et al (1999) Interaction of molecular oxygen with the vacuum-annealed TiO2 (110) surface: molecular and dissociative channels. J Phys Chem B 103:5328–5337. doi:10.1021/jp990655q
52. Kuznetsov VN (2002) Study of oxygen adsorption and reoxidation of reduced titanium dioxide by thermal desorption mass spectrometry. Kinet Catal 43:868–873
53. Haerudin H, Bertel S, Kramer R (1998) Surface stoichiometry of "titanium suboxide", part I volumetric and FTIR study. J Chem Soc Faraday Trans 94:1481–1487. doi:10.1039/a707714i